2026 IEEE International Conference on Robotics and Automation (ICRA 2026)
June 1-5, 2026. Vienna, Austria

Wirelessly Powered Zero Net Magnetic Torque Motor for Tissue Regenerating Robotic Implant

Jack GS Davies[1], Jialun Liu[1], Cameron Duffield[1], Zihan Zhao[1], Dana D Damian[1,2], and Shuhei Miyashita[1,2]

***Abstract*— In biomedical engineering, robotic implants have shown new methods to restore and improve bodily function and regenerate tissue. A significant challenge with the design of these devices is to safely actuate them for weeks or months while they reside in a patient's body. The application of a rotating magnetic field offers a solution to remotely transfer torque. However, this method will cause a net torque on the body within the field, which will cause rotational motion of the implant. Here we present a wirelessly-driven magnetic motor which can be driven with an external magnetic field, using an electromagnetic coil(s), to control a robotic implant. Due to the magnetic torque canceling mechanism, this wireless motor is actuatable with a single coil and produces no net torque on the entire body. When physically tested, the motor was able to produce around 0.5 mNm of torque, which is comparable to conventional ungeared motors of the same size. The motor was demonstrated in a robotic implant and successfully applied force to stretch a porcine esophagus.**

I. Introduction

Driven by the rapid growth of interdisciplinary advances, medical robots' *in vivo* operations have shown potential to revolutionize various fields of medicine. Surgical robots operating from outside of the body are widely clinically approved and are used to improve the outcomes of surgical interventions [1], [2]. Tethered crawlers have been shown to improve the effectiveness of certain procedures, such as colonoscopies [3]. Untethered robots, for example, the capsule endoscope, provide a new solution to gastrointestinal (GI) diseases, incorporating tiny wireless cameras and wireless actuation techniques [4], [5]. Not restricted to active visual imaging, medical robots *in vivo* have also shown promise in foreign matter retrieval [6], [7], targeted drug delivery [8], and ophthalmologic procedures [9]. Another area of interest is the use of robotic implants for long-term therapies. These devices can remain in the body and perform functions such as supporting heart function [10], performing as an artificial pancreas [11], and mechanostimulation-modulated tissue regeneration [12].

One of the significant challenges with designing robotic implants is power delivery and control [13]. Conventional motors require a source of electricity to run which could be provided by wires or inductively. However, there are inherent risks to running electricity through the body. Using magnetic fields to control devices wirelessly has been shown to be a plausible solution [14], and magnetic fields of up to 7 T are approved for use in MRI machines with no adverse effects on patients. Another challenge is how to minimize the net torque produced on the device's body. A torque can be applied on a magnetic dipole by rotating the external magnetic field [15], however, this will lead to a net torque on the whole body. Recent work has demonstrated a wirelessly actuated rotation-free magnetic motor, which achieves output torque without inducing net rotational motion on the entire device body, thereby addressing one of the major limitations of rotating-field actuation [16]. Ensemble control strategies have been applied to capsule robots, where oscillating external magnetic fields were used to independently actuate dual motors, enabling dexterous 2 degree-of-freedom (DOF) robotic arm motions with minimized body torque [17].

This paper presents a novel wirelessly-driven magnetic motor for use in robotic implants and *in vivo* medical robots. The motor uses a single or symmetric pair of external coils

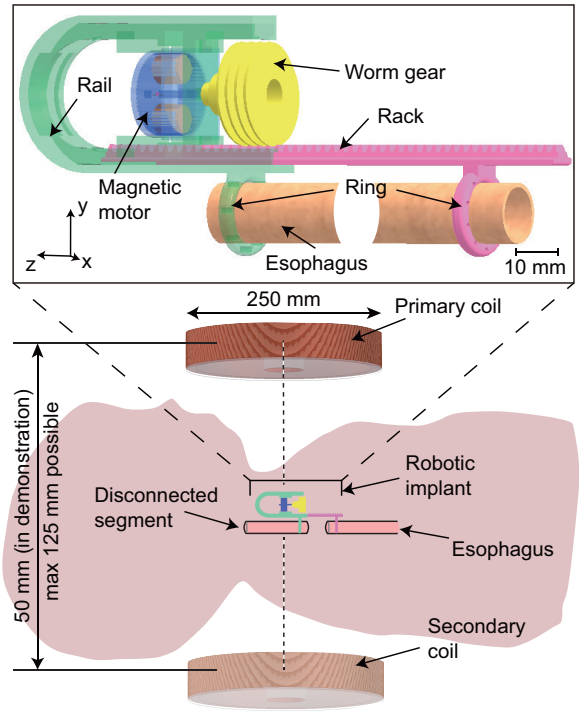

Fig. 1. **The developed wirelessly powered robotic implant.** This implant equipped with the proposed wireless magnetic motor, can lengthen tubular organs by applying a uniaxial force. The height of the implant rail is 36.25 mm and the length of the implant rack is 122.5 mm.

[1]The authors are with the Sheffield Microrobotics Lab, School of Electrical and Electronic Engineering, The University of Sheffield, Sheffield S1 3JD, UK. jialun.liu@sheffield.ac.uk
[2] Insigneo Institute for *in silico* Medicine, University of Sheffield, UK.

(Fig. 1) which generate an alternating magnetic field in a single plane to produce a useful output torque within the body of the motor. The implant does not experience a net torque around its entire body, and therefore, there is no overall rotating movement. The implant does not contain any electronic components such as a DC motor or battery.

This motor is demonstrated as incorporated in a device to lengthen tubular organs by applying a uniaxial force, advancing our previous work [18]. The device could be used to improve the treatment of esophageal atresia or short bowel syndrome. Esophageal atresia traditionally requires multi-week sedation and ventilation. Sutures attached to the esophagus are manually pulled from outside of the patient's body to adjust the tension in the esophagus [19]; this device has the potential to radically transform the current surgical conduit.

This paper introduces a new motor architecture when compared to our previous work in [20], relying on actuation by magnetic torque instead of force. The proposed design is driven on both directions of the oscillating magnetic field, increasing its rotational speed. This new design is able to perform the same task with a 64% reduction in magnet mass (reduction from 5 mm to 3 mm cubic magnets). Elimination of the ratchet mechanism reduces the moving part count to only 3 and facilitates further miniaturization. Additionally, when the driving magnetic field is absent, the motor can hold at a designated position with a smaller error than previous designs.

The contributions of the paper are:

1) Designing and developing a novel wireless motor architecture with constant output torque and no net torque on the whole body, using magnetic torque.
2) Modeling and testing the output torque of the motor and force of the implant incorporating the motor.
3) Testing and verifying the device with *ex vivo* esophageal tissue.

II. Methods

This section explains some of the design choices made and models the performance of the motor.

A. Requirements

In order for the motor to be useful, it should produce a constant torque over a cycle and not be back-drivable even when the magnetic field is absent. There should be no net torque applied to the whole body of the motor. The motor needs to be able to displace around 3 mm of tissue (this displacement is applied every 24 h to a patient's esophagus). While previous robotic implants for gastrointestinal tract regeneration have applied up to 2.5 N, the appropriate force to be applied to produce healthy tissue is still unknown.

B. Mechanism

The proposed motor uses the torque applied to a magnetic dipole within a magnetic field to generate a useful output torque. The motor shown in Fig. 2 uses a ratchet wheel and two pawls with two 3 mm cube neodymium magnets

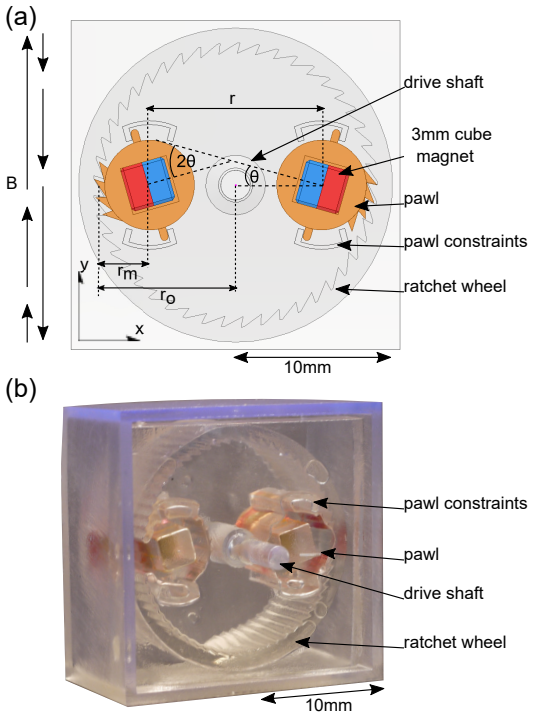

Fig. 2. **The developed wireless motor with direction of alternating magnetic flux density (B).** (a) Labeled diagram. (b) Manufactured motor.

installed. There is a 180° phase difference between each pawl. A drive shaft is located in the center. The field causes the pawls to rotate around their shafts in opposite directions due to their 180° phase difference (see Fig. 3). These pawls are used to drive the ratchet wheel in a single direction. The magnets in each pawl oppose, which causes the pawls to repel. The pawls are able to move away from each other slightly and engage on the ratchet wheel. This clearance allows the pawl to clear the ratchet wheel teeth when they are returning. The design allows 30° of rotation for the pawls. The maximum backlash in this design should be no more than half of this rotational limit of 30°, and in practice, should be less than half a tooth due to the positions that the pawls naturally rest in. This motor requires an external magnetic field that alternates directions in a single axis. The alternating magnetic field can be generated by a single coil or by a symmetric pair.

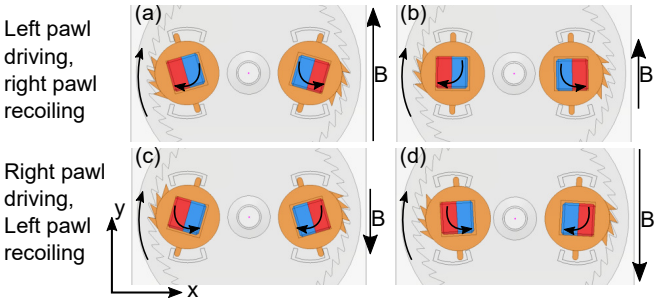

Fig. 3. **Motion of pawls and drive ratchet.** (a-b) Left pawl driving. (c-d) Right pawl driving.

The torque applied $\vec{\tau}$ to a magnetic dipole $\vec{m}$ given a magnetic flux density produced by an electromagnetic coil $\vec{B_c}$ is given by the cross product $\vec{m} \times \vec{B_c}$. We can simplify this expression for this particular application by:

1) Taking torque around the z axis (Fig. 2) and ignoring other torques, $\vec{\tau} = \begin{bmatrix} 0 & 0 & \tau \end{bmatrix}^\top$. This is the only axis the pawls are able to rotate around.
2) The coil system generates a field with only a y component, $\vec{B_c} = \begin{bmatrix} 0 & B_c & 0 \end{bmatrix}^\top$.
3) Ignoring z component of magnetic dipole moment, $\vec{m} = \begin{bmatrix} m_x & m_y & 0 \end{bmatrix}^\top$. The pawls are not able to rotate in a way which produces a z component.

C. Motor Torque

We define a variable θ which is the angle that an individual pawl makes with the x axis, $15° > \theta > -15°$. The torque on the pawl from a magnetic field τ_c given the magnetic flux density B_c is:

$$\tau_c = |\vec{m}|\, B_c \cos\theta. \tag{1}$$

This means that to keep torque as high and linear as possible, θ must be kept close to 0°. The design in Fig. 2 attempts to maximize the torque based on Eq. (1).

As one magnet is driving the ratchet wheel, there is another one resetting. As the magnets move simultaneously and are mirrored, the angle between the 2 pawls will be 2θ. The magnetic field generated by the resetting magnet B_m will interact with the driving pawl as the magnets are close together. There will be a torque applied τ_{int} between the 2 dipoles that opposes the torque from the coil [21]:

$$\tau_{int} = -\frac{\mu_0 |\vec{m}|^2}{2\pi r^3} \sin|2\theta|, \tag{2}$$

where r is the distance between two magnets, μ_0 is the permeability of free space. The resultant torque on the pawl τ_{pawl} is:

$$\tau_{pawl} = |\vec{m}|\, B_c \cos\theta - \frac{\mu_0 |\vec{m}|^2}{2\pi r^3} \sin|2\theta|. \tag{3}$$

Given that r_o is the radius of the ratchet wheel and r_m is the radius of the pawl attached to the magnet, the output torque τ_o of the motor is:

$$\tau_o = \tau_{pawl} \frac{r_0}{r_m}, \tag{4}$$

$$\tau_o = \frac{r_0}{r_m} \left(|\vec{m}|\, B_c \cos\theta - \frac{\mu_0 |\vec{m}|^2}{2\pi r^3} \sin|2\theta| \right). \tag{5}$$

Eq. (3) shows that to generate a useful amount of torque, the magnets should be sufficiently far apart from each other to reduce τ_{int}. This must be balanced with maintaining enough of an interaction to provide the repelling force that engages the pawls on the ratchet wheel. In order to model the torque profile of the motor, we need to evaluate: B_r, $\mu_0 |\vec{m}|$, and $\frac{r_0}{r_m}$, where B_r is the residual magnetic flux density of the material. Eq. (6) is used to find the approximate value of $|\vec{m}|$ using B_r = 1.3 T, which is taken from the magnet specifications and the volume of the permanent magnet V:

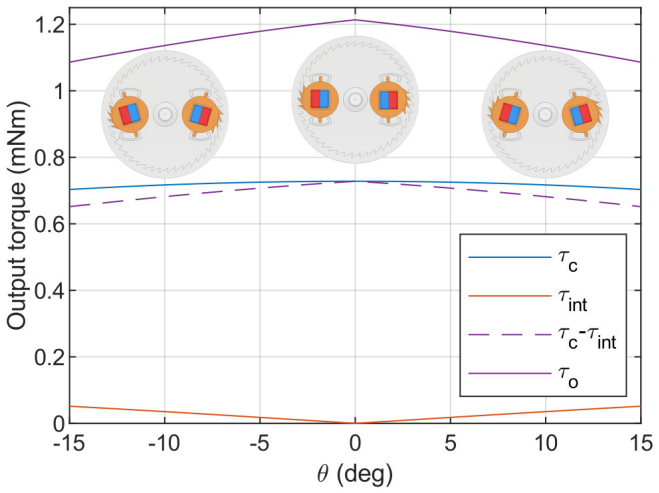

Fig. 4. **Simulated output torque profile for a pawl cycle.**

$$|\vec{m}| = \frac{1}{\mu_0} B_r V. \tag{6}$$

We estimated that the magnetic moment of the 3 mm neodymium cube magnets used is m = 0.0280 Am^2. The torque increase caused by the gear reduction between the pawl and the ratchet wheel is: $\frac{r_o}{r_m} = 1.67$.

Fig. 4 shows the simulated torque profile of a single pawl over its driving stroke. The maximum torque of 10.9 mNm is generated at $\theta = 0°$ and the minimum of 12.1 mNm is generated at $\theta = 15°$ either side of this. This torque profile could be further flattened by increasing the distance between the pawls; however, this reduces the force that engages them with the ratchet wheel. The resting position of the pawls will be at the ends of their travel ($-15°$ or $15°$). The start-up torque of the motor is dependent on the torque the motor is able to produce at this rest position. For the implant, start-up torque is the most important factor as it will move slowly, for short distances, and needs to be restarted multiple times.

The easiest way to increase torque is to increase B_c. The increased flux density has no effect on the strength of the internal interactions. An interesting effect of this is that the torque profile over a cycle (Fig. 4, τ_o) flattens as flux density increases, as the internal interactions become increasingly small compared to the torque from the external field. The coil system used for validating this motor is only able to achieve a maximum B_c of 26 mT; the model suggests that increasing the field strength will linearly increase torque and flatten the torque profile. Clinical MRI systems routinely sustain magnetic field strengths on the order of Teslas across air gaps significantly larger than those in our study. This shows it is possible to bring the power density of our design much closer to conventional motors with improvements to the coil design.

Another way to increase the torque of the motor is to increase the magnetic dipole moment of the pawls (Fig. 5). The pawls have space to, at least, double the mass of the

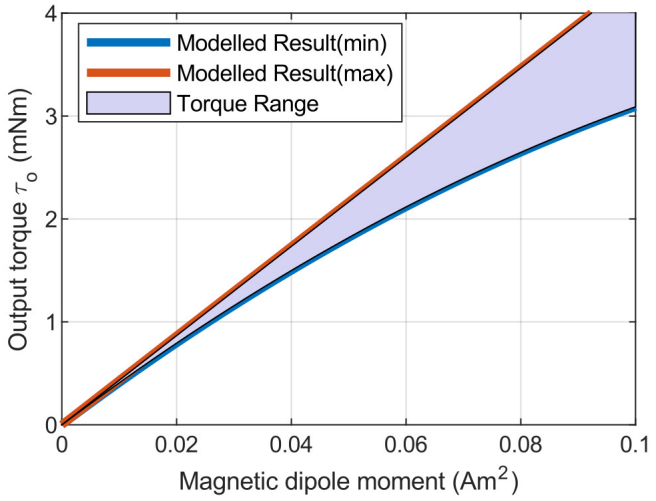

Fig. 5. **Simulated torque vs magnetic dipole moment.**

magnets which would effectively double $\vec{m}$. This model suggests that it would not increase torque linearly, and the torque profile will become less flat. Changing $\vec{m}$ would also change the force between the 2 magnets, which could impact the motor's function by increasing friction.

D. Motor Speed

The rotational speed of the motor depends on the frequency of the magnetic field. The coil system attempts to generate a square wave, and for each half wavelength, the pawls are able to move a maximum of one tooth. This means the pawls rotate 9° per half wavelength. Due to the gear reduction, the ratchet wheel will move approximately 11° for each full wavelength of the alternating magnetic field. This gives the relationship: $\omega_m = 0.03\,\omega_B$, where ω_B is the frequency of the magnetic field and ω_m is the angular velocity of the pawl.

We expect the motor to have a step-out frequency. This is due to the pawls needing a finite quantity of time in order to move through a full rotation. If the pawls are unable to achieve this movement before the field switches, the motor's speed will be significantly reduced. A model of magnetic step-out for rolling robots [22] can be adapted to approximate the behavior of the motor:

$$\omega_m = \begin{cases} 0.03\,\omega_B, & \omega_B \le \omega_{so} \\ 0.03\left(\omega_B - \omega_B\sqrt{1-\left(\frac{\omega_{so}}{\omega_B}\right)^2}\right), & \omega_B > \omega_{so} \end{cases} \tag{7}$$

where ω_{so} is the step-out frequency. The step-out frequency of the pawl can be found by finding the time it takes for the pawl to rotate through 30 degrees on the resetting stroke. Given the angle in radians θ and angular acceleration α the time this takes is:

$$t = \sqrt{\frac{2\theta}{\alpha}}. \tag{8}$$

Given the moment of inertia of the pawl around its axis of rotation $I = f(m, r)$, torque from the magnetic field, τ_m, and torque from dynamic friction, τ_f, the acceleration of the pawl is:

$$\alpha = \frac{\tau_c - \tau_f}{I}. \tag{9}$$

This gives us the step-out frequency as:

$$\omega_{so} = 2\pi\sqrt{\frac{2\theta I}{\tau_c - \tau_f}}. \tag{10}$$

E. Implant Force and Speed

The force and the linear speed of the implant can be derived from the torque and rotational speed of the motor. Let P be the total power of the drive system, then

$$P = \tau_o\,\omega_m = \eta\,F\,v, \tag{11}$$

where v is the moving speed of the rack, $\tau_o\omega_m$, $\eta F v$ represents the power from the worm gear and rack, respectively. η estimates the efficiency loss of the rack-worm gear transmission system, which is mainly caused by friction.

Given the tooth pitch k, we can find the force applied as:

$$F = \frac{1}{\eta}\frac{2\pi}{k}\tau_o \tag{12}$$

$$= \frac{1}{\eta}\frac{2\pi}{k}\frac{r_0}{r_m}(mB_c\cos\theta) - \frac{\mu_0 m^2}{2\pi r^3}\sin 2\theta), \tag{13}$$

where $k = \frac{2\pi\omega_m}{v}$. The moving speed of the rack is given by:

$$v = \frac{1}{\eta}\frac{\omega_m k}{2\pi}. \tag{14}$$

F. Fabrication and Experimental Setup

The motor and implant (worm gear, rack, and rail) were manufactured using a Form 2 SLA printer with 25 micron layer height. The parts were printed using Formlabs clear resin. Parts were secured with cyanoacrylate adhesive (LOCTITE). The moving parts were lubricated with WD-40 oil to reduce friction. The motor sits on a horizontal work bed between a pair of 250 mm diameter Helmholtz coils: the primary and secondary coil. The secondary coil is optional and is for boosting the strength of the magnetic field. The distance between the coils is 50 mm. The working surface is 12 mm above the primary coil and 40 mm below the secondary coil. When a current (maximum 10 A) runs on the coil, a vertical magnetic field is produced. By periodically reversing the current, we are able to get an alternating magnetic field. The frequency and flux density of this magnetic field are variable.

III. Results

A. Motor Torque Simulation and Experiment

The motor was placed on the work bed, and a piece of mono-filament nylon thread was glued to the output shaft. This thread ran around a pulley above the bed, and a mass of adhesive putty was suspended from it. More adhesive putty was added to the mass until the motor stalled. The mass was then weighed, and the experiment was repeated for a range of B_c.

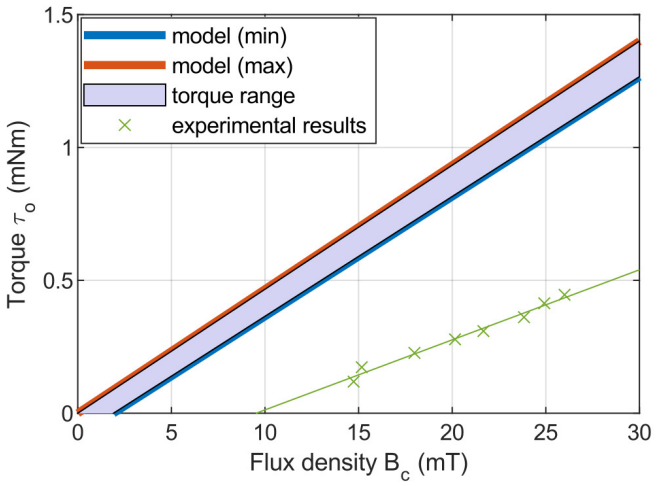

Fig. 6. **Torque vs flux density obtained in both simulations and experiments.**

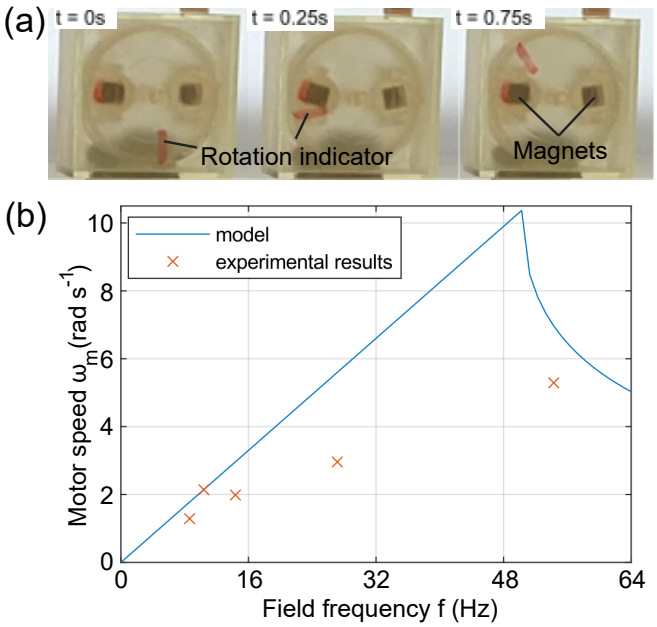

Fig. 7. **Motor speed characterization.** (a) Running the motor between 2 coils. The magnetic flux density is 26 mT. The red lines indicate the rotation of the motor. (b) Speed of motor over magnetic field frequency. The magnetic field frequency f in Herz equals to $\frac{\omega_B}{2\pi}$.

The model predicts that the torque of the motor will increase linearly with respect to flux density. The experimental results in Fig. 6 show this linear relationship; however, there is a lower torque than predicted. One reason for the gap between experimental results and the model is overcoming the friction between the pawl and ratchet wheel surfaces, which is not included in the idealized model. For the current prototype, the small feature size and tight tolerance requirements are approaching the limit of our SLA printing process. We expect to be able to achieve stronger agreement with the model with improved manufacturing techniques.

The model predicts that the motor only produces torque for a single component of the magnetic field. This was verified by placing the motor on its side; the motor did not drive the output shaft when placed in the wrong orientation. This means that multiple motors could be used in a device and selectively actuated by changing the direction of the alternating magnetic field.

B. Motor Speed Simulation and Experiment

The model predicts that the motor's rotational speed will increase linearly with increasing magnetic field frequency until it reaches the step-out frequency. The step-out frequency of the pawls was found by taking the time taken to retract the pawls from the videos taken. The speed of the motor was found by recording each test with 120 fps frame rate and timing at least one full rotation. Fig. 7 (a) shows the running motor, while fig. 7 (b) plots the simulated and experimental results.

The results are slightly lower than modeled. The observed discrepancy between the modeled and experimental results is largely attributed to the surface roughness and dimensional tolerances inherent in the SLA printing process at this scale. These imperfections increase dynamic friction thus the pawls were found to not engage on the ratchet around 10-20% of the time. These occasional pawl slippages could be mitigated through higher-precision micro-manufacturing techniques. Fig. 7 shows that the speed of the motor is seriously reduced when the field frequency is greater than $100\,\mathrm{rad{\cdot}s^{-1}}(16\,\mathrm{Hz})$. To assess whether the step-out model closely matches the real system behavior, more tests would need to be performed at higher frequencies.

Gap time is defined as the interval required for current reversal during the oscillation of the magnetic field, during which no magnetic field is present. A reduction in gap time results in a faster current switching rate. Under a constant oscillating field duration, shorter gap times are associated with higher motor rotational speeds. Fig. 8 illustrates the relationship between the time and frequency required for a single motor rotation with varying gap times ranging from 10 ms to 50 ms. For a gap time of 50 ms, the resulting relationship curves exhibit a clear and consistent trend. However, for gap times of 10 and 30 ms, pronounced fluctuations in the data are observed, which are mainly attributed to the inability of the pawl to complete its full rotational cycle.

C. Comparison with Conventional Motors

This section will compare the performance of the magnetic torque motor with two other conventional motors. The first motor used for comparison is the "Faulhaber Brushed DC Motor" from RS Components, as this is a similar size and shape. The second motor is the motor from the previous implant work [12], which is a 6 V motor with a 300:1 gearbox.

The maximum experimental torque of the magnetic motor is higher than the brushed DC motor and is of a similar size. The torque of the brushed DC motor would be difficult to increase as the windings are rated for a certain voltage/current. The torque generated by the magnetic motor scales with

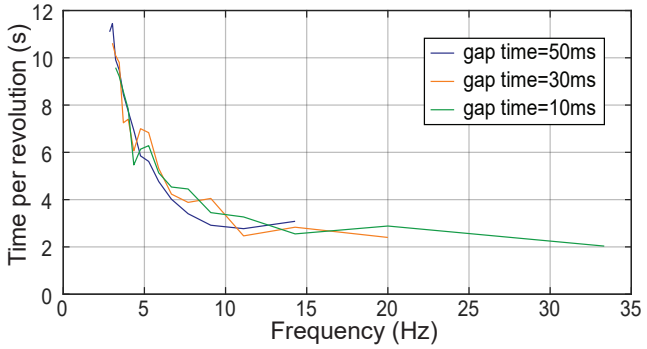

Fig. 8. **Motor speed in different gap times.** The three curves show the correlation between time and motor rotation frequency under gap times ranging from 10 ms to 50 ms.

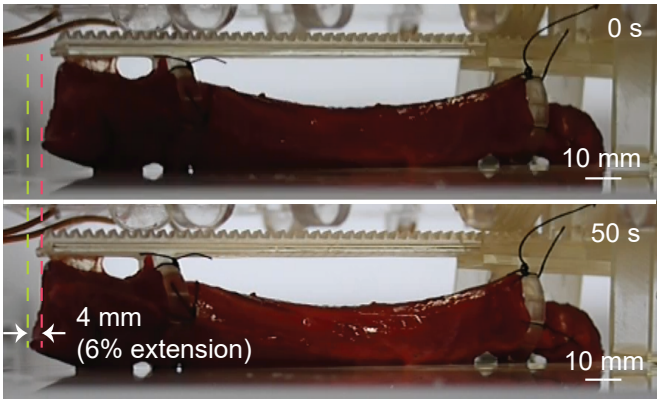

Fig. 9. **Implant stretching the porcine esophagus.** The start is represented by the red dashed line and the end result at t = 50 s is represented by the green dashed line.

the flux density of the external field and could be increased by using a more powerful coil system or larger magnets in the pawls. The speed of the magnetic motor is lower than conventional designs as it is limited by the step-out frequency of the pawls. A higher flux density will increase the step-out frequency; however, the speed of the motor is adequate for this application. The power consumption of the motor is dependent on the method used to generate the external magnetic field. The coil system used in this work used 240 W to generate the maximum flux density of 26 mT.

A conventional motor can generate heat when it runs, which is undesirable. The developed magnetic motor does not require any physical connections and can be powered from a distance, depending on the power of the electromagnetic coils used. The developed motor is not back-drivable, meaning that it does not require a brake mechanism if it is used in a robotic implant. Another advantage of this motor design is the scalability due to the simple design. It has been shown that magnetic torque scales favorably as size decreases compared with other powering methods [23].

D. Robotic Implant Ex Vivo Demonstration

We demonstrate the viability of using the remotely powered motor in the robotic implant to induce tissue growth. The robotic implant was first used to stretch one phantom tissue, fabricated from Ecoflex 00-30 (Smooth On Inc.), and then one porcine esophagus. For both trials, the implant was placed horizontally as shown in Fig. 9, between the two coils and was actuated with a strength of field of 26 mT, alternating at 3 Hz. First, the phantom tissue, measuring 115 mm in length and 82 mm^2 in cross-sectional area, was attached to the attachment rings using Sil-Poxy (Smooth On Inc.). The robotic implant was suspended with a string to the roof of the coil system, where the distance between the two attachment rings was 71 mm. The implant was able to stretch the phantom tissue 2.5 mm in 30 seconds (3.5% extension).

The implant was then used to stretch a porcine esophagus, which was sutured, with simple interrupted sutures, to the attachment rings of the implant (Fig. 9). The esophagus measured 100 mm in length and 11 mm in diameter when relaxed. The distance between the two attachment rings was 65 mm before stretching. The implant was able to stretch the tissue 4 mm in 50 seconds (6% extension). These results show that the robotic implant is able to successfully stretch materials comparable to those found within the body.

TABLE I

COMPARISON WITH CONVENTIONAL MOTORS

	Faulhaber brushed DC motor	**DC motor used in [12]**	**Presented wireless motor (experimental)**
Stall torque (mNm)	0.35	340 (with 300 :1 gearbox)	1
No-load speed (rad·s^{-1})	260	11.5	6
Power at stall torque (W)	0.35	9	Varies with magnetic drive system
Dimensions (mm)	Cylinder: ∅15, depth 10.5	$24.4 \times 12 \times 10$	Cylinder: ∅20, depth 10

IV. DISCUSSION & CONCLUSION

In this paper, we present a novel wirelessly actuated magnetic motor and its implementation in a robotic implant. A pair of electromagnetic coils powers the developed motor by utilizing the torque applied to a magnetic dipole within a magnetic field. With the coil system used in this setup, the motor was shown to produce comparable torque to a conventional DC motor. This style of motor has advantages over conventional motors and shows potential for use in robotic implants.

We estimate that the appropriate working distance between the two coils, for a typical baby, is approximately 20 cm. This value is greater than the distance we demonstrated in this paper; however, this is due to the limited strength of the applied magnetic field ($\leq$ 26 mT), which is capped by the maximum current that the current coil drivers and power sources can handle. The MRI machines routinely used in hospitals show that fields of 3 T (over 100 times stronger) are feasible and could extend the working range. The linear relationship between the coil current (and thus B_c) and the output torque provides a predictable method for remote

control. By modulating the frequency and magnitude of the coil current, clinicians can adjust the stretching force and speed in real-time without the need for onboard sensors or batteries.

With a permanent magnet installed on the rack, we would be able to find the stretching distance of the implant remotely. An array of Hall-effect sensors installed in the magnetic drive system would allow conducting magnetic localization for the installed implant [7].

Regarding scalability, reducing magnet size would decrease the magnetic dipole moment m cubically. However, since the output torque τ_o is proportional to $B_c m$, this reduction can be compensated for by increasing the external field B_c or by increasing the gear ratio of the internal worm gear. This scalability ensures that the device can be miniaturized for pediatric applications.

The optimal force needed to induce esophageal tissue growth via uniaxial mechanostimulation is unknown and has only been approximated in the past. We conclude that the force induced onto the tissue has the potential to induce tissue growth, even though a lower force is assumed compared to other papers [18]. In our ex vivo porcine esophagus demonstration, the implant achieved a $4\,\text{mm}$ extension within $50\,\text{seconds}$. This speed comfortably exceeds the clinical requirement of $2.5\,\text{mm}$ displacement per 24 hours, demonstrating the readiness of the motor for mechanostimulation therapies [12]. The future work includes testing over multiple hours, encoding of the action of the motor, and the improvement of the producible force of the implant with reduction gearing.

REFERENCES

[1] C. Bergeles and G.-Z. Yang, "From passive tool holders to microsurgeons: safer, smaller, smarter surgical robots," *IEEE Transactions on Biomedical Engineering*, vol. 61, no. 5, pp. 1565–1576, 2013.

[2] N. P. Wiklund, "Technology insight: surgical robots—expensive toys or the future of urologic surgery?" *Nature Clinical Practice Urology*, vol. 1, no. 2, pp. 97–102, 2004.

[3] M. C. Carrozza, L. Lencioni, B. Magnani, P. Dario, D. Reynaerts, M. G. Trivella, and A. Pietrabissa, "A microrobot for colonoscopy," in *MHS'96 Proceedings of the Seventh International Symposium on Micro Machine and Human Science*, 1996, pp. 223–228.

[4] S. Yim, K. Goyal, and M. Sitti, "Magnetically actuated soft capsule with the multimodal drug release function," *IEEE/ASME Transactions on Mechatronics*, vol. 18, no. 4, pp. 1413–1418, 2013.

[5] M. Nokata, S. Kitamura, T. Nakagi, T. Inubushi, and S. Morikawa, "Capsule type medical robot with magnetic drive in abdominal cavity," in *2008 2nd IEEE RAS EMBS International Conference on Biomedical Robotics and Biomechatronics*, 2008, pp. 348–353.

[6] S. Miyashita, S. Guitron, K. Yoshida, Shuguang Li, D. D. Damian, and D. Rus, "Ingestible, controllable, and degradable origami robot for patching stomach wounds," in *2016 IEEE International Conference on Robotics and Automation (ICRA)*, 2016, pp. 909–916.

[7] J. Liu, H. Sugiyama, T. Nakayama, and S. Miyashita, "Magnetic sensor based topographic localization for automatic dislocation of ingested button battery," in *2020 IEEE International Conference on Robotics and Automation (ICRA)*, 2020, pp. 5488–5494.

[8] B. P. Timko, T. Dvir, and D. S. Kohane, "Remotely triggerable drug delivery systems," *Advanced Materials*, vol. 22, no. 44, pp. 4925–4943, 2010.

[9] M. P. Kummer, J. J. Abbott, B. E. Kratochvil, R. Borer, A. Sengul, and B. J. Nelson, "Octomag: An electromagnetic system for 5-DOF wireless micromanipulation," *IEEE Transactions on Robotics*, vol. 26, no. 6, pp. 1006–1017, 2010.

[10] E. T. Roche, M. A. Horvath, I. Wamala, A. Alazmani, S.-E. Song, W. Whyte, Z. Machaidze, C. J. Payne, J. C. Weaver, and G. Fishbein, "Soft robotic sleeve supports heart function," *Science translational medicine*, vol. 9, no. 373, 2017.

[11] V. Iacovacci, L. Ricotti, P. Dario, and A. Menciassi, "Design and development of a mechatronic system for noninvasive refilling of implantable artificial pancreas," *IEEE/ASME Transactions on Mechatronics*, vol. 20, no. 3, pp. 1160–1169, 2015.

[12] D. D. Damian, K. Price, S. Arabagi, I. Berra, Z. Machaidze, S. Manjila, S. Shimada, A. Fabozzo, G. Arnal, D. Van Story, J. D. Goldsmith, A. T. Agoston, C. Kim, R. W. Jennings, P. D. Ngo, M. Manfredi, and P. E. Dupont, "In vivo tissue regeneration with robotic implants," *Science Robotics*, vol. 3, no. 14, 2018.

[13] G.-Z. Yang, J. Bellingham, P. E. Dupont, P. Fischer, L. Floridi, R. Full, N. Jacobstein, V. Kumar, M. McNutt, R. Merrifield, B. J. Nelson, B. Scassellati, M. Taddeo, R. Taylor, M. Veloso, Z. L. Wang, and R. Wood, "The grand challenges of science robotics," *Science Robotics*, vol. 3, no. 14, 2018.

[14] S. Miyashita, S. Guitron, S. Li, and D. Rus, "Robotic metamorphosis by origami exoskeletons," *Science Robotics*, vol. 2, no. 10, 2017.

[15] A. W. Mahoney and J. J. Abbott, "Generating rotating magnetic fields with a single permanent magnet for propulsion of untethered magnetic devices in a lumen," *IEEE Transactions on Robotics*, vol. 30, no. 2, pp. 411–420, 2014.

[16] U. U. Harman, A. Hafez, C. Duffield, Z. Zhao, L. Dixon, D. Rus, and S. Miyashita, "Wirelessly actuated rotation-free magnetic motor," in *2024 IEEE/RSJ International Conference on Intelligent Robots and Systems (IROS)*, 2024, pp. 2387–2393.

[17] Z. Zhao, A. Hafez, and S. Miyashita, "Ensemble control of a 2-dof parallel link arm in a capsule robot using oscillating external magnetic fields," in *2025 IEEE International Conference on Robotics and Automation (ICRA)*, 2025, pp. 9081–9087.

[18] D. D. Damian, S. Arabagi, A. Fabozzo, P. Ngo, R. Jennings, M. Manfredi, and P. E. Dupont, "Robotic implant to apply tissue traction forces in the treatment of esophageal atresia," in *2014 IEEE International Conference on Robotics and Automation (ICRA)*, 2014, pp. 786–792.

[19] J. E. Foker, T. C. Kendall Krosch, K. Catton, F. Munro, and K. M. Khan, "Long-gap esophageal atresia treated by growth induction: the biological potential and early follow-up results," *Seminars in pediatric surgery*, vol. 18, pp. 23–29, 2009.

[20] C. Duffield, A. F. Smith, D. Rus, D. Damian, and S. Miyashita, "Wirelessly magnetically actuated motor for tissue regeneration robotic implant," in *2022 IEEE/RSJ International Conference on Intelligent Robots and Systems (IROS)*, 2022, pp. 465–471.

[21] J. J. Abbott, E. Diller, and A. J. Petruska, "Magnetic methods in robotics," *Annual Review of Control, Robotics, and Autonomous Systems*, vol. 3, pp. 57–90, 2020.

[22] A. W. Mahoney, N. D. Nelson, K. E. Peyer, B. J. Nelson, and J. J. Abbott, "Behavior of rotating magnetic microrobots above the step-out frequency with application to control of multi-microrobot systems," *Applied Physics Letters*, vol. 104, no. 14, p. 144101, 2014.

[23] O. Cugat, J. Delamare, and G. Reyne, "Magnetic micro-actuators and systems (magmas)," *IEEE Transactions on magnetics*, vol. 39, no. 6, pp. 3607–3612, 2003.